International Communications in Heat and Mass Transfer 133 (2022) 105955

Contents lists available at ScienceDirect

International Communications in Heat and Mass Transfer

journal homepage: www.elsevier.com/locate/ichmt

Analysis of thermo-magnetic convection and entropy generation of Al_2O_3-water nanofluid in a partially heated wavy electronic cabinet

C. Sivaraj [a], S. Gowtham [a], M. Elango [b], M.A. Sheremet [c,*]

[a] Department of Mathematics, PSG College of Arts & Science, Coimbatore 641014, Tamil Nadu, India
[b] Department of Physics, PSG College of Arts & Science, Coimbatore 641014, Tamil Nadu, India
[c] Laboratory on Convective Heat and Mass Transfer, Tomsk State University, 634050 Tomsk, Russia

ARTICLE INFO

Keywords:
Entropy generation
Flush mounted heater
MHD
Nanosuspension
Thermal convection
Wavy cavity

ABSTRACT

A computational analysis has been performed to study the effect of magnetic parameter on magneto-natural convection and entropy generation inside a wavy cabinet filled by Al_2O_3-H_2O nanosuspension. The vertical boundaries of the cavity are designed as wavy and kept at cooled temperature (T_c), while the horizontal borders are modeled as flat and supposed to be thermally insulated except the centrally heated portion on the bottom wall. The higher constant temperature (T_h) of the isothermal line source can supply thermal energy in uniform manner. The transformed dimensionless governing equations were solved using finite volume technique along with power-law scheme. The system was optimized for significant variety of controlling parameters namely, number of undulations ($N = 0$–3), volume fraction of nanosuspension ($\phi = 0.0$–0.04), magnetic parameter ($Ha =$ 0 and 50), magnetic tilted angle ($\zeta = 0°$–90°) and dimensionless heat difference ($\Omega = 0.001$–0.1). The numerical results are analyzed for streamlines, isotherms, entropy isolines, overall Nusselt number and average entropy production strength. From this study, it is noticeable that growth of undulation number causes the reduction of convective heat transfer rate as well as average entropy production intensity. Further, the findings elucidate that the average entropy production intensity and overall heat transfer rate are decreased upon growing magnetic parameter.

1. Introduction

Magnetohydrodynamic (MHD) thermal convection within cavities is one of the prominent fields of investigation because of an extensive range of applications in numerous disciplines i.e., crystal growing in fluids, metal forming [1], plasma confinement, fluid metals, electromagnetic molding [2], coolants in nuclear reactor, turbulent controller [3], MHD thermal generator systems [4] etc. So far, numerical investigations have been reported in this fascinating area on magnetic natural convection in sealed enclosures [5], three-dimensional [6] and two-dimensional [7] chambers.

Wavy-walled chamber is one of the shapes used in several gadgets to improve their heat transfer efficiency. It is further difficult to set this kind of boundaries than that of flat surfaces like square or rectangular due to its greater area and consequently, larger surface allows to enhance thermal convection through energy exchange. The heat transfer in wavy cavities has been analyzed by various researchers owing to their vital applications in refrigerator [8], underground cable structures, molten core of the earth [9], solar energy collection and cooling structure [10]. Indeed, only very few investigations have been performed on thermal convection including magnetic impact inside wavy geometries. For example, Nasrin and Parvin [11] analyzed their problem of convection heat transfer inside a wavy chamber along with sinusoidally heated region including the transverse magnetic field. The authors reported that the overall heat transfer at the lower corrugated portion enhances with a raise of the number of wavy surfaces contrarily reduces with growing magnetic parameter. Asad et al. [12] analyzed the influence of undulations on magneto-natural convection heat transport in a vertical wavy enclosure with isothermal boundary conditions at the bottom wall. They reported that maximum value of undulations enhances the overall heat transfer rate than the square boundary.

Many authors devoted their work to study the wavy structured enclosures within heat sources located at discrete parts of the cavity [13,14]. Among them, lowermost heat source inside the chamber holds precise applications due to its improved convective heat transfer. In this respect, one should spend attention in defining the dimension and position of the heating source which play crucial role in the determination

* Corresponding author.
E-mail address: sheremet@math.tsu.ru (M.A. Sheremet).

https://doi.org/10.1016/j.icheatmasstransfer.2022.105955

Available online 1 March 2022

Nomenclature

Roman letters

A	Area of the cavity (m^2)
a	Wavy shape parameter
b	Contraction ratio of undulated wall
B_0	Magnitude of the uniform magnetic impact (N A^{-1} m^{-1})
C_p	Heat capacity (J kg^{-1} K^{-1})
g	Acceleration of the gravitational force (m s^{-2})
Ge	Gebhart number $Ge = g\beta_{bf}L/(C_p)_{bf}$
Ha	Magnetic parameter $Ha^2 = B_0{}^2L^2\sigma_{bf}/\mu_{bf}$
k	Heat conductivity (W m^{-1} K^{-1})
l	Length of the dimensional heat source (m)
L	Length of the wavy enclosure (m)
N	Number of undulations
Nu	Nusselt number
p	Pressure (N m^{-2})
P	Dimensionless pressure
Pr	Prandtl number $Pr = \nu_{bf}/\alpha_{bf}$
Ra	Rayleigh number $Ra = g\beta_{bf}\Delta TL^3/\nu_{bf}\alpha_{bf}$
$s_l{}^*$	Local entropy production (W K^{-1} m^{-3})
S_l	Dimensionless local entropy production
$S_{l,avg}$	Dimensionless average total entropy production
$s_{l,\ ff}{}^*$	Local entropy production due to liquid friction (W K^{-1} m^{-3})
$S_{l,ff}$	Dimensionless local entropy production due to liquid friction
$S_{l,ff,avg}$	Dimensionless average entropy production due to liquid friction
$s_{l,\ ht}{}^*$	Local entropy production due to thermal transfer (W K^{-1} m^{-3})
$S_{l,ht}$	Dimensionless local entropy production due to thermal transfer
$S_{l,ht,avg}$	Dimensionless average entropy production due to thermal transfer
$s_{l,\ mf}{}^*$	Local entropy production due to external magnetic impact (W K^{-1} m^{-3})
$S_{l,mf}$	Dimensionless local entropy production due to external magnetic impact
$S_{l,mf,avg}$	Dimensionless average entropy production due to external magnetic impact
T	Temperature (K)
t	Time (s)
T_h	Temperature at isothermal line source (K)
T_c	Temperature at cold vertical wavy borders (K)
u, v	Velocity components in x- and y- directions (m s^{-1})
U, V	Dimensionless velocity components in X- and Y- directions
x, y	Cartesian coordinates (m)
X, Y	Dimensionless Cartesian coordinates

Greek Symbols

α	Thermal diffusivity (m^2 s^{-1})
β	Parameter of thermal expansion (K^{-1})
μ	Dynamic viscosity (Pa s)
θ	Dimensionless temperature
ε	Dimensionless heat source length $\varepsilon = l/L$
χ	Irreversibility distribution ratio
ζ	Magnetic tilted angle
ρ	Density (kg m^{-3})
ν	Kinematic viscosity (m^2 s^{-1})
σ_{bf}	Electrical conductivity of the base liquid (S m^{-1})
σ_{nf}	Electrical conductivity of the nanosuspension (S m^{-1})
τ	Dimensionless time
ϕ	Volume fraction of nanoparticles
q_1, q_2, q_3, J	Geometrical coefficients
ω	Dimensionless vorticity
Ψ	Dimensionless stream function
Ω	Dimensionless temperature difference
ξ, η	Transformed Cartesian coordinates

Subscripts

avg	Average
bf	Base liquid
c	Cold
h	Hot
l	Local
nf	Nanosuspension
s	Solid

Superscript

*	Dimensional form

of the specific applications, namely, cooling of electronic devices, building heaters, meteorological melting of glasses and so on [15]. Also, a comprehensive review of natural convection in various types of enclosures under localized heating portions has been analyzed by Oztop et al. [16]. The authors examined the influences of type and location of heat sources as well as the effects of different configurations of cavities with various thermal boundary conditions. Further, Saha [17] investigated the thermo-magnetic convection in a sinusoidal corrugated enclosure with discrete isoflux heating on the bottom section. They showed that the average convective heat transfer decreases with increasing the heat source surface area.

Nanofluid is a medium which play a pivotal role in thermal transmission. When inclusion of nanoparticles along with traditional base liquids such as oil, ethylene glycol or H_2O form nanofluids which assist to improve the heat conductivity as well as convection and conduction processes due to its peculiar properties [18]. Accordingly, several reports have been drawn on standard liquids like air or H_2O in wavy domains associated with the process of free convection [19]. Besides, many researchers have been driven on this field and made their investigations on wide variety of nanoliquid applications [20–23] in biotechnological area [24] including plant cell walls for improved bio-fuel production [25] as well as chemical engineering, medical sections [26], chemotherapy [27] and microbial fuel cells [28]. Few authors have been explored their findings in the form of textbooks that are discussed about the fundamentals of nano liquids in wavy cavities [29,30]. In this context, Abu Nada and Oztop [31] investigated thermal transfer and flow field inside a wavy enclosure filled by Al_2O_3-H_2O nanosuspension. Cho et al. [32] studied thermal convection along a vertical undulated surface within alumina-water nanoliquid. Nikfar and Mahmoodi [33] numerically reported the problem on natural convection of nanoliquid inside a chamber with vertical wavy walls. From the investigations presented in [31–33] for the case of thermal convection along with two-sided wavy chambers and they reported that overall Nusselt number significantly improved with rising nanoadditives to the traditional base liquids inside the entire wavy domain. Further, MHD natural convection in a tilted wavy enclosure which is filled by copper-water nanoliquid including the corner heated portion was analyzed by Sheremet et al. [34] and they exposed that the average heat transfer enhances with growing nanoparticles together with base liquids. Also, a raise of the undulation parameter diminishes the convective flow rate, whereas increases the rate of heat transfer. Sheremet et al. [35] made a comprehensive study on free convective heat transfer within a top undulated

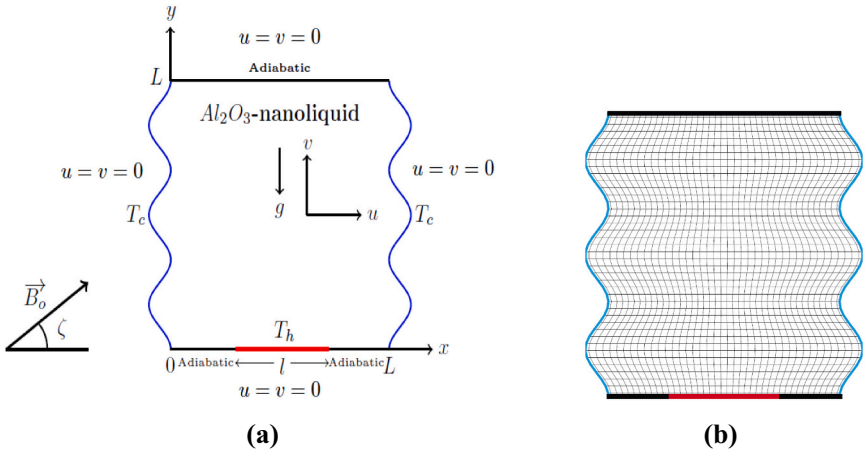

Fig. 1. (a): Geometry of the partially heated wavy cavity and (b): computational domain of the proposed model.

chamber of nanoliquid whose enclosure is equipped with left bottom heater. It is reported that convective liquid motion attenuates and Nusselt number significantly improved with the volumetric nanosuspension. Oztop et al. [36] studied the problem of magnetohydrodynamic (MHD) combined convection in a nanofluid flow in a partially heated wavy-walled enclosure. They discovered that the temperature gradient was reduced by raising a volume fraction of nanoparticles. Sheremet et al. [37] analyzed a problem on natural convection within a tilted wavy chamber filled by Al_2O_3-water nanoliquid together with the process of non-uniform heating and they found that the Nusselt number value can be reduced upon increasing volume fraction of nanoliquid for all given values of cavity inclination angles. Uddin et al. [38] scrutinized the magnetic natural convection of nanoliquid within a square domain inside upper corrugated wall. The study ascertains that the influence of magnetic parameter and its inclination angle control the Nusselt number and significant reduction of heat transfer rate when Hartmann parameter decreases. More recently, experimental analysis of Al_2O_3-H_2O nanofluid simulation was explored by Chen et al. [39]. They concluded that thermogravitational convection of nanofluids is greatly enhanced by the electrical field, which improvements of voltage and concentration.

To improve an energy process, it is essential to minimize the entropy production owing to their thermal transfer, liquid friction and magnetic impact irreversibilities [40–42]. Accordingly, Oztop and Salem [43] have studied an extensive review on entropy production in mixed and thermal convection for energy classifications. Also, entropy production owing to thermal transfer and liquid motion of nanoliquid inside different geometries was reviewed theoretically and numerically by Mahian et al. [44]. In addition, various researchers have reported on thermal convection and entropy production within flat surface or complex geometries filled by base liquid (H_2O) or air [45]. In this regard, Cho [46] scrutinized the impact of thermal convection and entropy production inside a partially heated undulated enclosure filled by Al_2O_3-H_2O nanoliquid. The author predicted from the analysis that the heat transfer phenomena and average entropy production increase with growth of *Ra* for all given Al_2O_3-nanoadditives. A numerical analysis of entropy production and free convection of *Cu*-H_2O nanoliquid in a vertical wavy chamber was investigated by Kashani et al. [47]. They found that Nusselt number and entropy production can be decreased with increasing nanoparticles concentration. Bhardwaj et al. [48] examined the convective heat transfer as well as entropy production inside a triangular chamber with left wavy boundary. They reported that thermal entropy production is the same for both undulation and without undulation surfaces. Moreover, liquid friction entropy production is significantly enhanced for undulation parameters than that of no undulation. Parveen and Mahapatra [49] numerically investigated the problem of entropy production in double-diffusive thermal convection within a top undulated chamber filled by alumina-water nanoliquid with a heater at the bottom zone and they concluded that augmentation of *Ra* raises the total entropy production rate. Further, the development of number of undulations, buoyancy ratio and magnetic parameter diminish the total entropy generation strength. Further, thermal convection and entropy production of Al_2O_3-H_2O nanosuspension in a crown wavy chamber was analyzed by Dogonchi et al. [50]. Recently, Munawar et al. [51] considered the analysis of entropy generation on natural convective heat transfer in a corrugated triangular annulus filled by hybrid nanofluid with a central triangular heater. They reported that the overall entropy generation significantly affects upon the inner triangular body is heated at uniform or non-uniform temperature. Other related investigations can be found in Refs. [52–54].

The above-detailed review of literature manifests that a numerical study of thermal convection and entropy production within a wavy chamber filled by Al_2O_3-H_2O nanoliquid is an essential study to unveil some salient results. However, there is no study was reported which analysis the entropy production and natural convection of alumina-H_2O nanoliquid inside a wavy chamber with a heated portion mounted on the lower boundary together with magnetic horizontal impact. The main goal of our present study is to improve convective heat transfer process and fluid flow patterns as well as minimizing entropy production of the entire chamber. Further, the novel design of wavy cavity and its varying parametrization pave path for the fabrication of cooling systems for electronic gadgets, electrical machineries and heat exchangers. Therefore, due to its practical interest in the engineering fields, the topic needs to be further explored.

2. Mathematical formulation

2.1. Schematic model explanation

The present work demonstrates laminar, 2D and natural convection process within a wavy chamber of length *L* which is portrayed in Fig. 1. An isothermal line source of length *l* is located at centre of the lowermost horizontal border. The vertical wavy boundaries are kept at low temperature T_c, whilst the horizontal flat surfaces of the chamber are assumed thermally adiabatic except the heating point. The enclosure boundaries can be considered as rigid and impermeable. The vertical boundaries of the wavy shape are defined by the following relations:

$$f_1(y) = L - L\left[a + b{\cdot}cos\left(2\pi N\frac{y}{L}\right)\right] \text{ and } f_2(y) = L\left[a + b{\cdot}cos\left(2\pi N\frac{y}{L}\right)\right] \quad (1)$$

where *a*, *b* and *N* represent the wavy shape, contraction ratio of the undulated wall and number of undulations respectively, and $a + b = 1$.

Table 1
Thermo-physical properties of the base liquid (H_2O) and nanoparticle (Al_2O_3) [61].

Physical Properties	H_2O	Al_2O_3
C_p [J kg^{-1} K^{-1}]	4179	765
ρ [kg m^{-3}]	997.1	3970
k [W m^{-1} K^{-1}]	0.613	40
β × 10^{-5} [K^{-1}]	20.7	0.85
σ [S m^{-1}]	0.05	10^{-10}
μ [kg m^{-1} s^{-1}]	0.001003	–
Pr	6.2	–

The wavy chamber is filled with Al_2O_3-H_2O nanoliquid which is presumed to be Newtonian and incompressible. Table 1 shows the thermo-physical properties of base liquid (H_2O) and nanoparticles (alumina). It is assumed that density is considered to be constant other than buoyancy term in which the Boussinesq approximation is applicable. It is also noticed that nanoparticles associated with base liquid are in thermal equilibrium. A uniform magnetic impact of strength B_0 disturbs the thermal and flow field pattern inside the chamber with an oblique angle of ζ to the horizontal plane. Moreover, the magnetic Reynolds number can be considered to be very small such that the induced magnetic impact is neglected compared to horizontal magnetic effect. Further, radiation and the viscous dissipation are also supposed to be negligible.

2.2. Dimensional governing equations

For the above-mentioned hypotheses, the governing equations are expressed in terms of dimensional Cartesian coordinates as follows [55–57]:

$$\frac{\partial u}{\partial x}+\frac{\partial v}{\partial y}=0 \tag{2}$$

$$\rho_{nf}\left(\frac{\partial u}{\partial t}+u\frac{\partial u}{\partial x}+v\frac{\partial u}{\partial y}\right)=-\frac{\partial p}{\partial x}+\mu_{nf}\left(\frac{\partial^2 u}{\partial x^2}+\frac{\partial^2 u}{\partial y^2}\right)+\sigma_{nf}B_o{}^2[v\cdot cos(\varsigma)-u\cdot sin(\varsigma)]sin(\varsigma) \tag{3}$$

$$\rho_{nf}\left(\frac{\partial v}{\partial t}+u\frac{\partial v}{\partial x}+v\frac{\partial v}{\partial y}\right)=-\frac{\partial p}{\partial y}+\mu_{nf}\left(\frac{\partial^2 v}{\partial x^2}+\frac{\partial^2 v}{\partial y^2}\right)+(\rho\beta)_{nf}g(T-T_c)+\sigma_{nf}B_o{}^2[u\cdot sin(\varsigma)-v\cdot cos(\varsigma)]cos(\varsigma) \tag{4}$$

$$\left(\rho C_p\right)_{nf}\left(\frac{\partial T}{\partial t}+u\frac{\partial T}{\partial x}+v\frac{\partial T}{\partial y}\right)=k_{nf}\left(\frac{\partial^2 T}{\partial x^2}+\frac{\partial^2 T}{\partial y^2}\right) \tag{5}$$

The initial and boundary conditions can be expressed as:

$$t=0: u=v=0, T=T_c, \text{at } 0\le x\le L \text{ and } 0\le y\le L, \tag{6}$$

$$t>0: u=v=0, T=T_c, \text{at } x=f_1(y) \text{ and } 0\le y\le L, \tag{7}$$

$$u=v=0, T=T_c, \text{at } x=f_2(y) \text{ and } 0\le y\le L, \tag{8}$$

$$u=v=0, \partial T/\partial y=0 \text{ at } y=L \text{ and } 0<x<L, \tag{9}$$

$$u=v=0, \partial T/\partial y=0 \text{ at } y=0 \text{ and } 0<x<(L-l)/2, (L+l)/2<x<L, \tag{10}$$

$$u=v=0, T=T_h, \text{at } (L-l)/2\le x\le (L+l)/2 \tag{11}$$

2.3. Physical properties of alumina-water nanoliquid

The effective density (ρ_{nf}) of the alumina-water nanoliquid is approximated by Pak and Cho correlation [58] as follows:

$$\rho_{nf}=(1-\phi)\rho_{bf}+\phi\rho_s \tag{12}$$

The specific heat $(\rho C_p)_{nf}$ is given by Xuan and Roetzel [59] as:

$$\left(\rho C_p\right)_{nf}=(1-\phi)\left(\rho C_p\right)_{bf}+\phi\left(\rho C_p\right)_s \tag{13}$$

The dynamic viscosity (μ_{nf}) of the nanoliquid is specified from Brinkman's correlation [60] as:

$$\mu_{nf}=\frac{\mu_{bf}}{(1-\phi)^{2.5}} \tag{14}$$

The thermal expansion coefficient (β_{nf}) can be expressed by [56]:

$$\beta_{nf}=(1-\phi)\beta_{bf}+\phi\beta_s \tag{15}$$

By using the Maxwell-Garnets (MG) model [56], the effective thermal conductivity (k_{nf}) of the nanoliquid can be defined as:

$$k_{nf}=k_{bf}\frac{k_s+2k_{bf}-2\phi\left(k_{bf}-k_s\right)}{k_s+2k_{bf}+\phi\left(k_{bf}-k_s\right)} \tag{16}$$

From the Maxwell model [56], the electrical conductivity (σ_{nf}) of the nanoliquid can be represented as:

$$\frac{\sigma_{nf}}{\sigma_{bf}}=1+\frac{3\left(\frac{\sigma_s}{\sigma_{bf}}-1\right)\phi}{\left(\frac{\sigma_s}{\sigma_{bf}}+2\right)-\left(\frac{\sigma_s}{\sigma_{bf}}-1\right)\phi} \tag{17}$$

The thermal diffusivity (α_{nf}) of the nanoliquid is formulated as follows:

$$\alpha_{nf}=\frac{k_{nf}}{\left(\rho C_p\right)_{nf}} \tag{18}$$

2.4. Dimensionless governing equations

In the present numerical approach, the pressure term has been eliminated from Eqs. (3) and (4) following the vorticity-stream function formulation. Further, the dimensionless variables are introduced as follows:

$$X=\frac{x}{L},\ Y=\frac{y}{L},\ U=\frac{uL}{\alpha_{bf}},\ V=\frac{vL}{\alpha_{bf}},\ P=\frac{pL^2}{\rho_{nf}\alpha_{bf}{}^2},\ \tau=\frac{t\alpha_{bf}}{L^2},\ \theta=\frac{T-T_c}{\Delta T},\ \Delta T=T_h-T_c \tag{19}$$

Therefore, the governing Eqs. (2)–(5) can be rewritten in dimensionless form by introducing

$$U=\frac{\partial \Psi}{\partial Y},\quad V=-\frac{\partial \Psi}{\partial X}\quad \text{and}\quad \omega=\frac{\partial V}{\partial X}-\frac{\partial U}{\partial Y} \tag{20}$$

as follows:

$$\frac{\partial^2 \Psi}{\partial X^2}+\frac{\partial^2 \Psi}{\partial Y^2}=-\omega \tag{21}$$

$$\frac{\partial \omega}{\partial \tau}+U\frac{\partial \omega}{\partial X}+V\frac{\partial \omega}{\partial Y}=\left(\frac{\mu_{nf}\rho_{bf}}{\mu_{bf}\rho_{nf}}\right)Pr\left[\frac{\partial^2 \omega}{\partial X^2}+\frac{\partial^2 \omega}{\partial Y^2}\right]+\left(\frac{\beta_{nf}}{\beta_{bf}}\right)RaPr\frac{\partial \theta}{\partial X}+\left(\frac{\sigma_{nf}\rho_{bf}}{\sigma_{bf}\rho_{nf}}\right)Ha^2Pr\left[\frac{\partial U}{\partial X}sin(\varsigma)cos(\varsigma)-\frac{\partial V}{\partial X}cos^2(\varsigma)-\frac{\partial V}{\partial Y}sin(\varsigma)cos(\varsigma)+\frac{\partial U}{\partial Y}sin^2(\varsigma)\right] \tag{22}$$

$$\frac{\partial \theta}{\partial \tau}+U\frac{\partial \theta}{\partial X}+V\frac{\partial \theta}{\partial Y}=\frac{\alpha_{nf}}{\alpha_{bf}}\left[\frac{\partial^2 \theta}{\partial X^2}+\frac{\partial^2 \theta}{\partial Y^2}\right] \tag{23}$$

The respective dimensionless parameters are defined as:

$$Pr=\frac{\nu_{bf}}{\alpha_{bf}},\quad Ra=\frac{g\beta_{bf}\Delta TL^3}{\nu_{bf}\alpha_{bf}},\quad Ha=B_0L\sqrt{\frac{\sigma_{bf}}{\mu_{bf}}},\quad \varepsilon=\frac{l}{L} \tag{24}$$

The corresponding dimensionless form of initial and boundary conditions can be represented as follows:

$$\tau = 0 : \Psi = \omega = 0, \theta = 0 \text{ at } 0 \le X \le 1 \text{ and } 0 \le Y \le 1, \tag{25}$$

$$\tau > 0 : \Psi = 0, \theta = 0, \omega = -\frac{\partial^2 \Psi}{\partial X^2} \text{ at } X = F_1(Y) = 1 - [a + b{\cdot}cos(2\pi NY)\,] \text{ and } 0 \le Y \le 1 \tag{26}$$

$$\Psi = 0, \theta = 0, \omega = -\frac{\partial^2 \Psi}{\partial X^2} \text{ at } X = F_2(Y) = a + b{\cdot}cos(2\pi NY) \text{ and } 0 \le Y \le 1 \tag{27}$$

$$\Psi = 0, \frac{\partial \theta}{\partial Y} = 0, \omega = -\frac{\partial^2 \Psi}{\partial Y^2} \text{ at } Y = 1 \text{ and } 0 < X < 1 \tag{28}$$

$$\Psi = 0, \frac{\partial \theta}{\partial Y} = 0, \omega = -\frac{\partial^2 \Psi}{\partial Y^2} \text{ at } Y = 0 \text{ and } 0 < X < \frac{1-\varepsilon}{2} \text{ and } \frac{1+\varepsilon}{2} < X < 1 \tag{29}$$

$$\Psi = 0, \theta = 1, \omega = -\frac{\partial^2 \Psi}{\partial Y^2} \text{ at } Y = 0 \text{ and } \frac{1-\varepsilon}{2} \le X \le \frac{1+\varepsilon}{2} \tag{30}$$

2.5. Average heat transfer rate

The convective heat transfer rate from the heat source to the neighbouring nanoliquid can be calculated by defining the dimensionless local Nusselt number as

$$Nu_l = -\left(\frac{k_{nf}}{k_{bf}}\right)\frac{\partial \theta}{\partial Y} \tag{31}$$

The average Nusselt number along the heated portion is expressed as

$$Nu_{avg} = \frac{1}{\varepsilon}\int_{(1-\varepsilon)/2}^{(1+\varepsilon)/2} Nu_l(X)dX \tag{32}$$

2.6. Entropy generation

In this present study, local entropy production is owing to the irreversibility nature of thermal transfer, liquid friction and magnetic impact. In Cartesian coordinates, the dimensional local entropy production is the addition of entropy production owing to thermal transfer, liquid friction and magnetic impact which is specified in the following form [55,62]

$$s_l^* = \frac{k_{nf}}{T^2}\left[\left(\frac{\partial T}{\partial x}\right)^2 + \left(\frac{\partial T}{\partial y}\right)^2\right] + \frac{\mu_{nf}}{T}\left[2\left(\frac{\partial u}{\partial x}\right)^2 + 2\left(\frac{\partial v}{\partial y}\right)^2 + \left(\frac{\partial u}{\partial y} + \frac{\partial v}{\partial x}\right)^2\right] + B_0^2\frac{\sigma_{nf}}{T}[u{\cdot}sin(\varsigma) - v{\cdot}cos(\varsigma)\,]^2 \tag{33}$$

where the first term is identified as local entropy production owing to thermal transfer ($s_{l,\ ht}^*$), the second term denotes the local entropy production owing to liquid friction ($s_{l,\ ff}^*$) and the third one expresses the local entropy production owing to magnetic impact ($s_{l,\ mf}^*$).

Applying the dimensionless variables specified in Eq. (19), the dimensional local entropy production can be converted to dimensionless form as follows

$$S_l = s_l^*\frac{{T_c}^2 L^2}{k_{bf}\Delta T^2} = S_{l,ht} + S_{l,ff} + S_{l,mf} \tag{34}$$

$$S_{l,ht} = \frac{k_{nf}}{k_{bf}}\frac{1}{\Omega^2\left(\theta + \Omega^{-1}\right)^2}\left[\left(\frac{\partial \theta}{\partial X}\right)^2 + \left(\frac{\partial \theta}{\partial Y}\right)^2\right] \tag{35}$$

$$S_{l,ff} = \frac{\mu_{nf}}{\mu_{bf}}\frac{1}{\Omega^2\left(\theta + \Omega^{-1}\right)}\frac{Ge}{Ra}\left[2\left(\frac{\partial U}{\partial X}\right)^2 + 2\left(\frac{\partial V}{\partial Y}\right)^2 + \left(\frac{\partial U}{\partial Y} + \frac{\partial V}{\partial X}\right)^2\right] \tag{36}$$

$$S_{l,mf} = \frac{\sigma_{nf}}{\sigma_{bf}}\frac{1}{\Omega^2\left(\theta + \Omega^{-1}\right)}\frac{Ge}{Ra}Ha^2[U{\cdot}sin(\varsigma) - V{\cdot}cos(\varsigma)\,]^2 \tag{37}$$

where

$$\Omega = \frac{\Delta T}{T_c} \text{ and } Ge = \frac{g\beta_{bf}L}{(C_p)_{bf}} \tag{38}$$

The dimensionless total entropy production ($S_{l,\ avg}$) can be found by integrating the local entropy production over the whole chamber which are expressed as follows

$$S_{l,ht,avg} = \frac{\iint_A S_{l,ht}\,dA}{\iint_A dA}, \quad S_{l,ff,avg} = \frac{\iint_A S_{l,ff}\,dA}{\iint_A dA}, \quad S_{l,mf,avg} = \frac{\iint_A S_{l,mf}\,dA}{\iint_A dA} \tag{39}$$

3. Numerical procedure

For the present numerical problem, the wavy enclosure is a physical domain in X and Y plane which is transformed into a rectangle computational geometry by using an algebraic coordinate transformation in terms of new independent coordinates ξ and η as below

$$\begin{aligned} X &= X(\xi, \eta) \\ Y &= Y(\xi, \eta) \end{aligned} \tag{40}$$

The basic enclosure geometry is mapped as rectangle computational geometry in Eq. (40) as follows

$$\begin{aligned} X &= \xi\,[F_2(Y) - F_1(Y)\,] + F_1(Y) \\ Y &= \eta \end{aligned} \tag{41}$$

After the transformation, the governing dimensionless Eqs. (21)–(23) can now be rewritten in the form of (ξ,η)

$$\left\{\frac{\partial}{\partial \xi}\left[\frac{1}{J}\left(q_1\frac{\partial \Psi}{\partial \xi} - q_2\frac{\partial \Psi}{\partial \eta}\right)\right] + \frac{\partial}{\partial \eta}\left[\frac{1}{J}\left(-q_2\frac{\partial \Psi}{\partial \xi} + q_3\frac{\partial \Psi}{\partial \eta}\right)\right]\right\} + \omega{\cdot}J = 0 \tag{42}$$

$$J\frac{\partial \omega}{\partial \tau} + \overline{U}\frac{\partial \omega}{\partial \xi} + \overline{V}\frac{\partial \omega}{\partial \eta} = \left(\frac{\mu_{nf}\rho_{bf}}{\mu_{bf}\rho_{nf}}\right)Pr\left\{\begin{array}{l}\frac{\partial}{\partial \xi}\left[\frac{1}{J}\left(q_1\frac{\partial \omega}{\partial \xi} - q_2\frac{\partial \omega}{\partial \eta}\right)\right] \\ +\frac{\partial}{\partial \eta}\left[\frac{1}{J}\left(-q_2\frac{\partial \omega}{\partial \xi} + q_3\frac{\partial \omega}{\partial \eta}\right)\right]\end{array}\right\} + \left(\frac{\beta_{nf}}{\beta_{bf}}\right)Ra\,Pr\left[\frac{\partial \theta}{\partial \xi}\frac{\partial Y}{\partial \eta} - \frac{\partial \theta}{\partial \eta}\frac{\partial Y}{\partial \xi}\right] + \left(\frac{\sigma_{nf}\rho_{bf}}{\sigma_{bf}\rho_{nf}}\right)Ha^2\,Pr\left\{\begin{array}{l}\left[\frac{\partial U}{\partial \xi}\frac{\partial Y}{\partial \eta} - \frac{\partial U}{\partial \eta}\frac{\partial Y}{\partial \xi}\right]sin(\varsigma)cos(\varsigma) - \left[\frac{\partial V}{\partial \xi}\frac{\partial Y}{\partial \eta} - \frac{\partial V}{\partial \eta}\frac{\partial Y}{\partial \xi}\right]cos^2(\varsigma) - \\ -\left[\frac{\partial V}{\partial \eta}\frac{\partial X}{\partial \xi} - \frac{\partial V}{\partial \xi}\frac{\partial X}{\partial \eta}\right]sin(\varsigma)cos(\varsigma) + \left[\frac{\partial U}{\partial \eta}\frac{\partial X}{\partial \xi} - \frac{\partial U}{\partial \xi}\frac{\partial X}{\partial \eta}\right]sin^2(\varsigma)\end{array}\right\} \tag{43}$$

$$J\frac{\partial\theta}{\partial\tau}+\overline{U}\frac{\partial\theta}{\partial\xi}+\overline{V}\frac{\partial\theta}{\partial\eta}=\frac{\alpha_{nf}}{\alpha_{bf}}\left\{\frac{\partial}{\partial\xi}\left[\frac{1}{J}\left(q_1\frac{\partial\theta}{\partial\xi}-q_2\frac{\partial\theta}{\partial\eta}\right)\right]+\frac{\partial}{\partial\eta}\left[\frac{1}{J}\left(-q_2\frac{\partial\theta}{\partial\xi}+q_3\frac{\partial\theta}{\partial\eta}\right)\right]\right\} \tag{44}$$

where

$$\overline{U}=\left[U\frac{\partial Y}{\partial\eta}-V\frac{\partial X}{\partial\eta}\right],\quad \overline{V}=\left[V\frac{\partial X}{\partial\xi}-U\frac{\partial Y}{\partial\xi}\right],\quad q_1=\left(\frac{\partial X}{\partial\eta}\right)^2+\left(\frac{\partial Y}{\partial\eta}\right)^2,$$

$$q_2=\left[\frac{\partial X}{\partial\xi}\frac{\partial X}{\partial\eta}+\frac{\partial Y}{\partial\xi}\frac{\partial Y}{\partial\eta}\right],\quad q_3=\left(\frac{\partial X}{\partial\xi}\right)^2+\left(\frac{\partial Y}{\partial\xi}\right)^2,\quad J=\left[\frac{\partial X}{\partial\xi}\frac{\partial Y}{\partial\eta}-\frac{\partial Y}{\partial\xi}\frac{\partial X}{\partial\eta}\right]$$

The new computational boundary conditions for the above case are:

$$\Psi=0,\theta=0,\omega=-\frac{q_1}{J^2}\frac{\partial^2\Psi}{\partial\xi^2}\ \text{on}\ \xi=0,1\ \text{and}\ 0\le\eta\le1 \tag{45}$$

$$\Psi=0,\frac{\partial\theta}{\partial\eta}=\frac{q_2}{q_3}\frac{\partial\theta}{\partial\xi},\omega=-\frac{q_3}{J^2}\frac{\partial^2\Psi}{\partial\eta^2}\ \text{on}\ \eta=1\ \text{and}\ 0<\xi<1 \tag{46}$$

$$\Psi=0,\frac{\partial\theta}{\partial\eta}=\frac{q_2}{q_3}\frac{\partial\theta}{\partial\xi},\omega=-\frac{q_3}{J^2}\frac{\partial^2\Psi}{\partial\eta^2}\ \text{on}\ \eta=1\ \text{and}\ 0<\xi<\frac{1-\varepsilon}{2},\quad\frac{1+\varepsilon}{2}<\xi<1 \tag{47}$$

$$\Psi=0,\theta=1,\omega=-\frac{q_3}{J^2}\frac{\partial^2\Psi}{\partial\eta^2}\ \text{on}\ \eta=0\ \text{and}\ \frac{1-\varepsilon}{2}\le\xi\le\frac{1+\varepsilon}{2} \tag{48}$$

The local Nusselt number can be rewritten in terms of new coordinates as follows

$$Nu_l=-\frac{k_{nf}}{k_{bf}}\left[\frac{-1}{J\sqrt{q_3}}\left(q_3\frac{\partial\theta}{\partial\eta}-q_2\frac{\partial\theta}{\partial\xi}\right)\right] \tag{49}$$

The average Nusselt number can be approximated as

$$Nu_{avg}=\frac{1}{\varepsilon}\int_{(1-\varepsilon)/2}^{(1+\varepsilon)/2}Nu_l(\xi)d\xi \tag{50}$$

The respective dimensionless Eqs. (35)–(37) of local entropy production caused by thermal transfer, liquid friction and magnetic impact can be written in new coordinates as below

$$S_{l,ht}=\frac{k_{nf}}{k_{bf}}\frac{1}{\Omega^2\left(\theta+\Omega^{-1}\right)^2}\left\{\left[\frac{1}{J}\left(\frac{\partial Y}{\partial\eta}\frac{\partial\theta}{\partial\xi}-\frac{\partial Y}{\partial\xi}\frac{\partial\theta}{\partial\eta}\right)\right]^2+\left[\frac{1}{J}\left(\frac{\partial X}{\partial\xi}\frac{\partial\theta}{\partial\eta}-\frac{\partial X}{\partial\eta}\frac{\partial\theta}{\partial\xi}\right)\right]^2\right\} \tag{51}$$

$$S_{l,ff}=\frac{\mu_{nf}}{\mu_{bf}}\frac{1}{\Omega^2\left(\theta+\Omega^{-1}\right)}\frac{Ge}{Ra}\left\{\begin{array}{l}2\left[\frac{1}{J}\left(\frac{\partial Y}{\partial\eta}\frac{\partial U}{\partial\xi}-\frac{\partial Y}{\partial\xi}\frac{\partial U}{\partial\eta}\right)\right]^2+2\left[\frac{1}{J}\left(\frac{\partial X}{\partial\xi}\frac{\partial V}{\partial\eta}-\frac{\partial X}{\partial\eta}\frac{\partial V}{\partial\xi}\right)\right]^2+\\+\left[\frac{1}{J}\left(\frac{\partial X}{\partial\xi}\frac{\partial U}{\partial\eta}-\frac{\partial X}{\partial\eta}\frac{\partial U}{\partial\xi}\right)+\frac{1}{J}\left(\frac{\partial Y}{\partial\eta}\frac{\partial V}{\partial\xi}-\frac{\partial Y}{\partial\xi}\frac{\partial V}{\partial\eta}\right)\right]^2\end{array}\right\} \tag{52}$$

$$S_{l,mf}=\frac{\sigma_{nf}}{\sigma_{bf}}\frac{1}{\Omega^2\left(\theta+\Omega^{-1}\right)}\frac{Ge}{Ra}Ha^2[U\cdot sin(\zeta)-V\cdot cos(\zeta)]^2 \tag{53}$$

The set of partial differential Eqs. (42)–(44) with their boundary conditions (45)–(48) has been solved by the finite volume method along with developed an in-house Fortran 90 code. In the finite volume technique, two essential things are considered i.e., the computational domain can be divided into finite number of control volumes in a uniform spacing and over this control volume, integration process has been done to convert the governing equations into the discretized equations. For the momentum and energy equations, the convective terms were employed with the power law differencing scheme, whilst diffusion terms were solved using the second order central differencing scheme. Moreover, the resulting set of discretized linear algebraic equations is solved based on a line-by-line procedure of the tri-diagonal matrix algorithm (TDMA). Further, the solution is obtained when the following convergence criteria of 10^{-7} is satisfied for all the variables (i.e., Ψ, ω or θ).

$$\frac{\left|\gamma_{i,j}^{n}-\gamma_{i,j}^{n-1}\right|}{\left|\gamma_{i,j}^{n}\right|}\le10^{-7} \tag{54}$$

Here the superscript n and subscripts i, j are given iteration parameter and space coordinates, respectively.

4. Code validation and grid independence

Validation is carried out in order to examine the accuracy, in which average Nusselt number at heated wavy portion is compared with the data of Nikfar and Mahmoodi [33]. The comparative results have been shown in Table 2 and it is noticed that the present algorithm is good with the prevailing result. Also, the Rayleigh number was fixed as $Ra=10^6$ for the validation.

The study of thermal convection in flat surfaces having lowermost heated centred region is investigated to scrutinize the numerical algorithm. Present analysis was performed with the computations of Calcagni et al. [63] and Aydin and Yang [64]. The obtained results are presented in Table 3 and it is found that the agreement is satisfactory.

Comparison of Nu_{avg} for numerous Ha and for a fixed value of $Ra=10^5$ and $\phi=0.04$ is presented in Table 4, in order to validate the results with Ghasemi et al. [65]. It is clearly identified that the obtained agreement is very close to the previous published results. Also, maximum deviation of observed parameter is about 1%.

The numerical model has been further validated using the outcomes of Magherbi et al. [66] and Cho et al. [67] in the situation of total entropy production. Table 5 shows varying of average entropy production rate for numerous values of Rayleigh numbers (Ra) as well as irreversibility distribution ratio (χ). It is observed that the present results match very well.

To scrutinize the grid independence of the simulation, a grid assessment was obtained for two cases along with the impact of undulation parameter (N), where case I and case II represent $\phi=0$, $Ha=0$ and $\phi=0$ & 0.04, $Ha=50$, $\zeta=0^\circ$ respectively which have shown in Table 6 and Table 7. Rest of the parameters are fixed as $Ra=10^6$ and $\varepsilon=0.5$. Average Nusselt number at the line source is monitored for the grid sizes of 82 × 82, 122 × 122, 162 × 162 and 202 × 202 elements. It is understood that the maximum variance between the appropriate grids is less than 2%. Hence the mesh of 162 × 162 elements is adopted for all the numerical simulations.

Table 2
Validation on average Nusselt number with previous analysis of Nikfar and Mahmoodi [33] (ϕ – nanoparticle volume fraction).

	ϕ = 0%	ϕ = 1%	ϕ = 4%
Present outcomes	7.7165	7.7803	7.9609
Nikfar and Mahmoodi [33]	7.606	7.685	7.931

Table 3
Comparison of current outcomes for Nu_{avg} with the literature in the case of flat surface model with ε = 0.8 (ε – heat source length in dimensionless parameter).

	$Ra = 10^4$	$Ra = 10^5$	$Ra = 10^6$
Present study	4.001	6.469	11.872
Calcagni et al. [63]	4.0	6.3	12.0
Aydin & Yang [64]	3.9	6.2	11.3

Table 4
The obtained Nu_{avg} related with the data of Ghasemi et al. [65].

	$Ha = 0$	$Ha = 30$	$Ha = 60$
Present Study	4.884	3.105	1.806
Ghasemi et al. [65]	4.896	3.124	1.815

Table 5
Comparison of arrived results with previously investigated by Magherbi et al. [66] and Cho et al. [67].

	$Ra = 10^3$		$Ra = 10^4$		$Ra = 10^5$
	$\chi = 10^{-1}$	$\chi = 10^{-2}$	$\chi = 10^{-2}$	$\chi = 10^{-3}$	$\chi = 10^{-3}$
Present results	35.54	4.56	105.22	12.54	190.59
Magherbi et al. [66]	35.62	4.56	104.05	12.50	193.96
Cho et al. [67]	35.62	4.57	105.35	12.55	191.79

Table 6
Test for grid independence for case I at $Ra = 10^6$, ε = 0.5, ϕ = 0 and $Ha = 0$ for different N.

N	Nu_{avg}			
	82 × 82	122 × 122	162 × 162	202 × 202
0	18.3862	18.0155	17.8842	17.8246
1	18.1834	17.8334	17.7116	17.6571
2	18.0612	17.7334	17.6237	17.5766
3	18.0722	17.7410	17.6358	17.5937

Table 7
Grid study of average Nusselt number for case II at $Ra = 10^6$, ε = 0.5, $Ha = 50$ and ζ = 0° for different values of N and ϕ.

N	ϕ	Nu_{avg}			
		82 × 82	122 × 122	162 × 162	202 × 202
0	0	15.5888	15.2817	15.1733	15.1269
	0.04	16.9240	16.6138	16.5047	16.4572
1	0	15.5917	15.2894	15.1840	15.1406
	0.04	16.9231	16.6185	16.5130	16.4682
2	0	15.6496	15.3687	15.2743	15.2362
	0.04	16.9864	16.7048	16.6115	16.5731
3	0	15.7169	15.4607	15.3815	15.3512
	0.04	17.0387	16.7848	16.7084	16.6801

5. Results and discussion

In the present investigation, the influence of inclined magnetic thermal convection and entropy production of Al_2O_3-H_2O nanoliquid is analyzed within a wavy cavity having an isothermal line source at lower border. The computations were carried out for the above system with Rayleigh number ($Ra = 10^6$), length of the line source (ε = 0.5), Prandtl number ($Pr = 6.2$), nanoparticles volume fraction (ϕ = 0.0–0.04), shape of the wavy ($a = 1.05$), number of undulations (N = 0–3), magnetic parameter (Ha = 0 and 50), magnetic tilted angle (ζ = 0°–90°) and the dimensionless temperature difference (Ω = 0.001–0.1). The Gebhart number (Ge) was calculated through the parameters Ra, Ω and fixed cooled border temperature of T_c = 300 K. For example, the values of Gebhart number take 3.05×10^{-8} for Ω = 0.001 and 1.41×10^{-8} for Ω = 0.01. The obtained results representing the behaviour of heat transfer, flow field and entropy contours are presented in terms of temperature pattern, stream function, average Nusselt numbers and local entropy production owing to thermal transfer, liquid friction and magnetic impact.

Fig. 2 shows the influence of undulation number N on the contours of isotherm, streamlines, local entropy production under the thermal transfer and liquid friction at ϕ = 0.04, $Ha = 0$ and Ω = 0.01. It is clearly manifest that the structure of thermal and flow fields is symmetric with respect to the vertical mid-line of the cavity. This is caused by symmetrical boundary conditions of the cooled vertical borders and isothermally partial heated portion of the designed cavity. Moreover, the crowded isotherm patterns close to the line source indicate the higher magnitude of temperature gradients prevailing there which in turn produce the heat plume over the line source.

Two symmetric counter rotating strong convective zones are manifested within the chamber and lines are parallel to the vertical boundaries when the absence of magnetic field is acted inside the enclosure. One can find that the vortices are formed inside centre of the cavity and it elongates in vertical direction. The flow is affected by waviness of the side walls, increment in N from zero (flat wall) to nonzero (wavy wall) boundary, the distorted isotherm patterns are observed inside the mid-portion of the chamber. This is owing to the fact that a wavy shape and an increase in length of cooled portion make the fluid particles to flow freely along the vertical wall and to cool effectively. For $N = 1$, a strong convective fluid flow is promoted within the cavity which can be seen in the values of $|\Psi|_{\max}$ (see Table 8). A further increase in N creates an obstruction effect in downward fluid motion resulted in the reduction of fluid velocity. The local entropy production caused by thermal transfer presented in Fig. 2(c) is concentrated at edges of the line source where the temperature gradient is presented, which is due to maximum heat transfer in those regions. It is understood that thermal entropy production is found to be less significant when the undulation number is increased. The patterns of liquid friction entropy production show the significant variation for distinct undulation numbers. For $N \leq 1$, the contour lines appear to be denser along the vertical walls and above the line source which indicate the high velocity gradients in this area. Interestingly, the existence of buoyancy force occurring in the edges of the line source and frictional force at the interacting edges of the counter rotating cells produces the entropy lines at those regions. When $N > 1$, the intensity of local entropy production caused by liquid friction near both the vertical boundaries and line source gets diminished. It is reasoned that the corrugated portion of the vertical walls slows down the fluid velocity within the cavity and hence reduces the velocity gradients.

The influence of magnetic parameter along with the inclination angle ζ = 0° is illustrated in Fig. 3 for ϕ = 0.04, Ha = 50, Ω = 0.01 and different undulation parameter N. It is seen from isotherms that the inclusion of magnetic field makes the upper part of the cavity with more thermally active and augments the thermal boundary layer thickness. From streamline contours, the strength of the convective fluid flow within the wavy chamber gets weakened and the significant changes in the vortex shape are observed. Moreover, when the magnetic parameter ($Ha = 50$) is applied to the horizontal direction, the Lorentz force creates the more attenuation effect in the vertical flow, shifting the core region of vortices downwards and hence the fluid particles deviate from the vertical centre line of the cavity. Thus, fluid particles fall smoothly along the vertical walls and the thin momentum boundary layer near the vertical walls. With the increasing number of undulations, we found that slightly varying convective cells are formed within the cavity that

supports the effective convective fluid flow rate. It is to be further noted from Table 8 that the maximum $|\Psi|_{max}$ value is obtained for $N = 1$ in the case of $Ha = 0$ whereas it occurs at $N = 2$ in the case of $Ha = 50$. From Fig. 3(c) and (d), a significant change in the liquid friction entropy production can be observed than the thermal entropy production when the magnetic impact is considered. It should be pointed out that inclusion of the magnetic field ($Ha = 50$) reduces the liquid friction entropy lines due to less velocity gradient.

When $N \geq 2$, the fluid flow along the vertical wavy walls experiences the effects of the attenuation from the Lorentz force and obstruction of the wavy shape, which produces low thickness of velocity boundary layers and hence more liquid friction entropy lines there. Fig. 3(e) reveals the contours of entropy generation owing to the presence of horizontal magnetic impact. Since the magnetic effect is applied horizontally, the intensity of Lorentz force is higher in the vertical direction and lower in the horizontal direction. Hence the magnetic entropy lines are prominent on the vertical flow regions such as near the vertical walls and vertical mid-line of the cavity. We further noticed the highest rate of magnetic entropy generation occurs above the heat source where the two recirculating convective cells with high velocity gradient interacts each other.

Table 8
Maximum values of stream function, local entropy production caused by thermal transfer, liquid friction and magnetic impact at $\Omega = 0.01$, $\phi = 0.04$ and different values of N, Ha and ζ.

N	Ha	ζ	$\lvert\Psi\rvert_{max}$	$S_{l,ht,max}$	$S_{l,ff,max}$	$S_{l,mf,max}$
0	0		41.1047	10,579.1	$2.0033{\cdot}10^{-4}$	–
	50	0°	12.0026	8960.42	$8.2024{\cdot}10^{-5}$	$7.3706{\cdot}10^{-5}$
		45°	17.7618	9741.14	$1.4433{\cdot}10^{-4}$	$3.8912{\cdot}10^{-5}$
		90°	18.7191	9378.42	$1.3702{\cdot}10^{-4}$	$4.3602{\cdot}10^{-5}$
1	0		44.3452	10,227.4	$1.8001{\cdot}10^{-4}$	–
	50	0°	12.4382	8893.78	$7.9048{\cdot}10^{-5}$	$7.6319{\cdot}10^{-5}$
		45°	18.1307	9753.55	$1.1896{\cdot}10^{-4}$	$4.0904{\cdot}10^{-5}$
		90°	18.0677	9308.88	$1.3708{\cdot}10^{-4}$	$4.3367{\cdot}10^{-5}$
2	0		39.7658	9936.86	$3.2423{\cdot}10^{-4}$	–
	50	0°	12.7172	8952.43	$9.2486{\cdot}10^{-5}$	$7.8665{\cdot}10^{-5}$
		45°	18.3960	9696.98	$2.4923{\cdot}10^{-4}$	$4.5318{\cdot}10^{-5}$
		90°	18.2220	9157.12	$2.7851{\cdot}10^{-4}$	$4.3024{\cdot}10^{-5}$
3	0		41.1185	10,088.3	$5.2517{\cdot}10^{-4}$	–
	50	0°	12.4359	9124.47	$1.3161{\cdot}10^{-4}$	$7.8270{\cdot}10^{-5}$
		45°	18.5881	9639.67	$2.9270{\cdot}10^{-4}$	$5.1943{\cdot}10^{-5}$
		90°	18.1397	9044.32	$4.1678{\cdot}10^{-4}$	$4.2735{\cdot}10^{-5}$

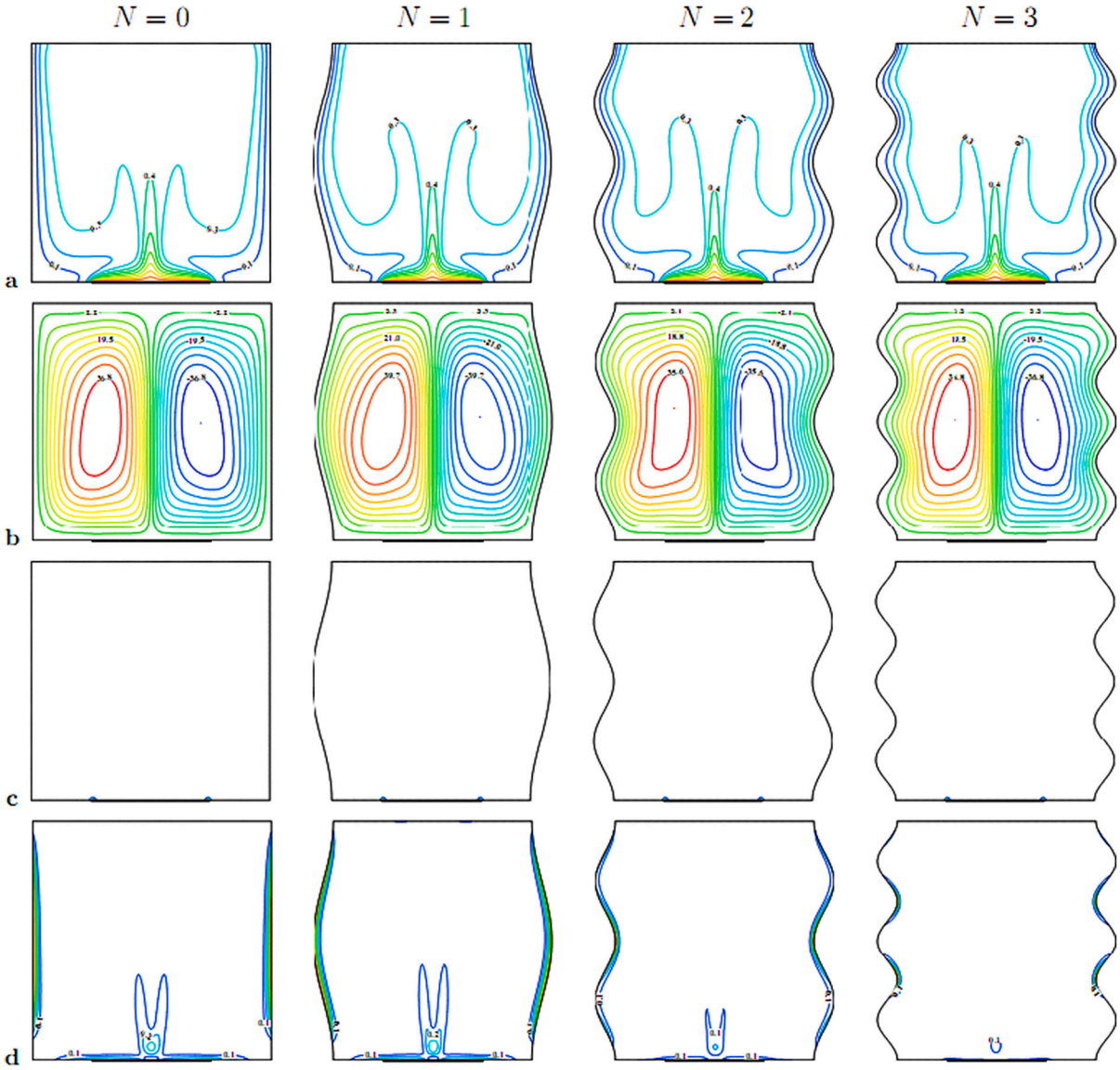

Fig. 2. θ (a), Ψ (b), $S_{l,ht}$ (c) and $S_{l,ff}$ (d) for $\phi = 0.04$, $Ha = 0$ and $\Omega = 0.01$ with different values of N.

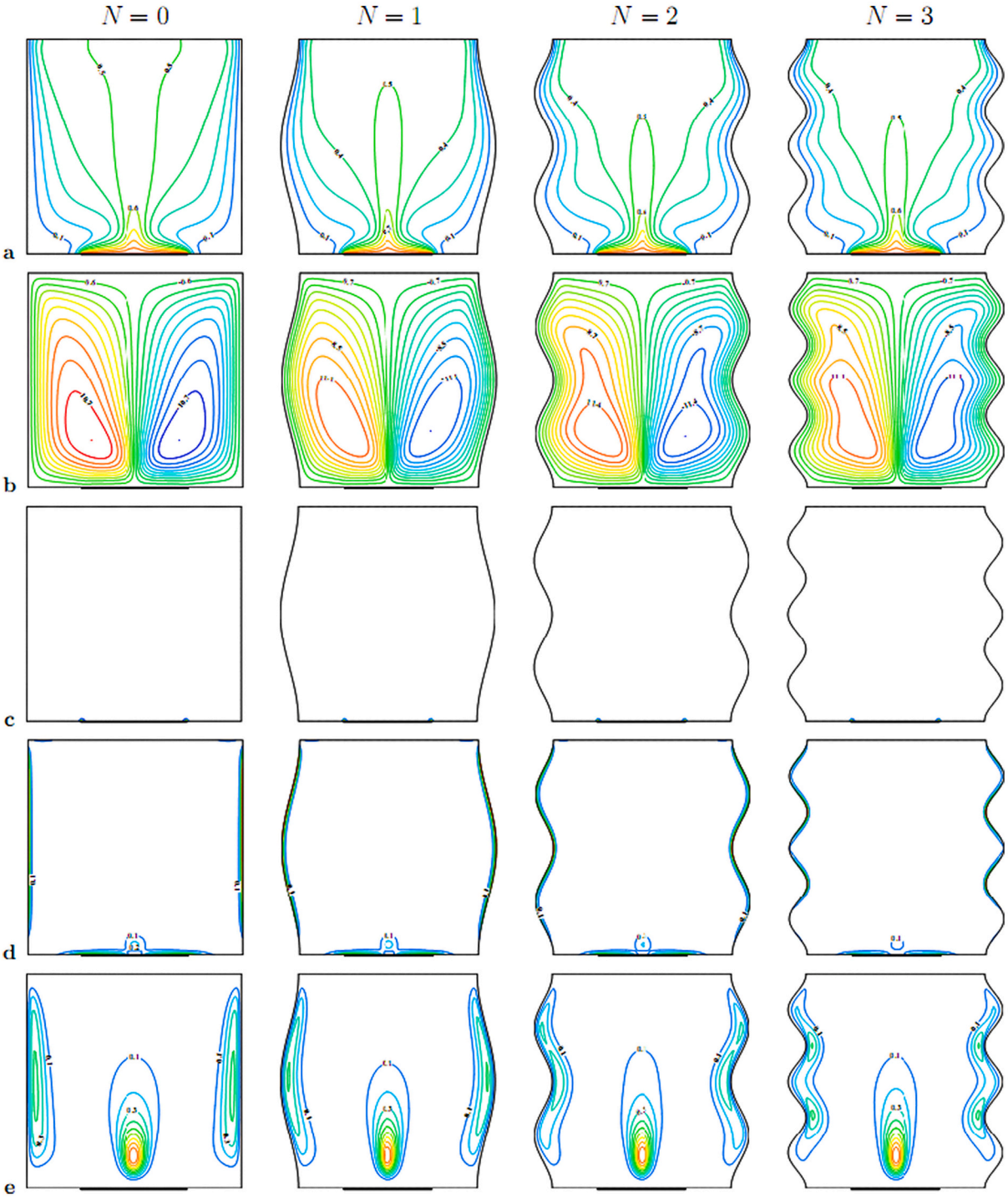

Fig. 3. θ (a), Ψ (b), $S_{l,ht}$ (c), $S_{l,ff}$ (d) and $S_{l,mf}$ (e) for $\phi = 0.04$, $Ha = 50$, $\zeta = 0^{\circ}$ and $\Omega = 0.01$ with different values of N.

Fig. 4 presents streamlines, isotherms and entropy parameters for various values of N at $\phi = 0.04$, $Ha = 50$, $\zeta = 45^{\circ}$ and $\Omega = 0.01$. Inclined Lorentz force distorts the symmetric form of isolines within the cavity by pushing the heat plume towards the right cold boundary. Upon increasing undulation parameter ($N > 2$), a greater magnitude of convective cell appears in the vicinity of uppermost portion of the enclosure (see Table 8). The thermal entropy production is primarily confined at ends of the bottom-line source and the liquid frictional contours are diminished significantly near both the cooled vertical walls and above the lower line source for all values of N (see Fig. 4c and d). Further, it is noticed that the magnetic entropy lines are highly intensified at vertical regions and over the line source and it is clear that observed pattern is operated by the applied horizontal magnetic field. When $N \geq 1$, crucial and extremely recirculating magnetic entropy lines are generated within the cavity (particularly at the corrugated portions), which is due to the hindrance effect is acted upon increasing undulation numbers. From streamlines pattern, counter clockwise rotating weaker cells are found to be shifted from core region of vortices. Physically, the significant change is manifested through applying the horizontal magnetic field resulting for higher rate of heat removed in the vicinity of the cooled right border.

The impact of undulation parameter of N on the patterns of thermal,

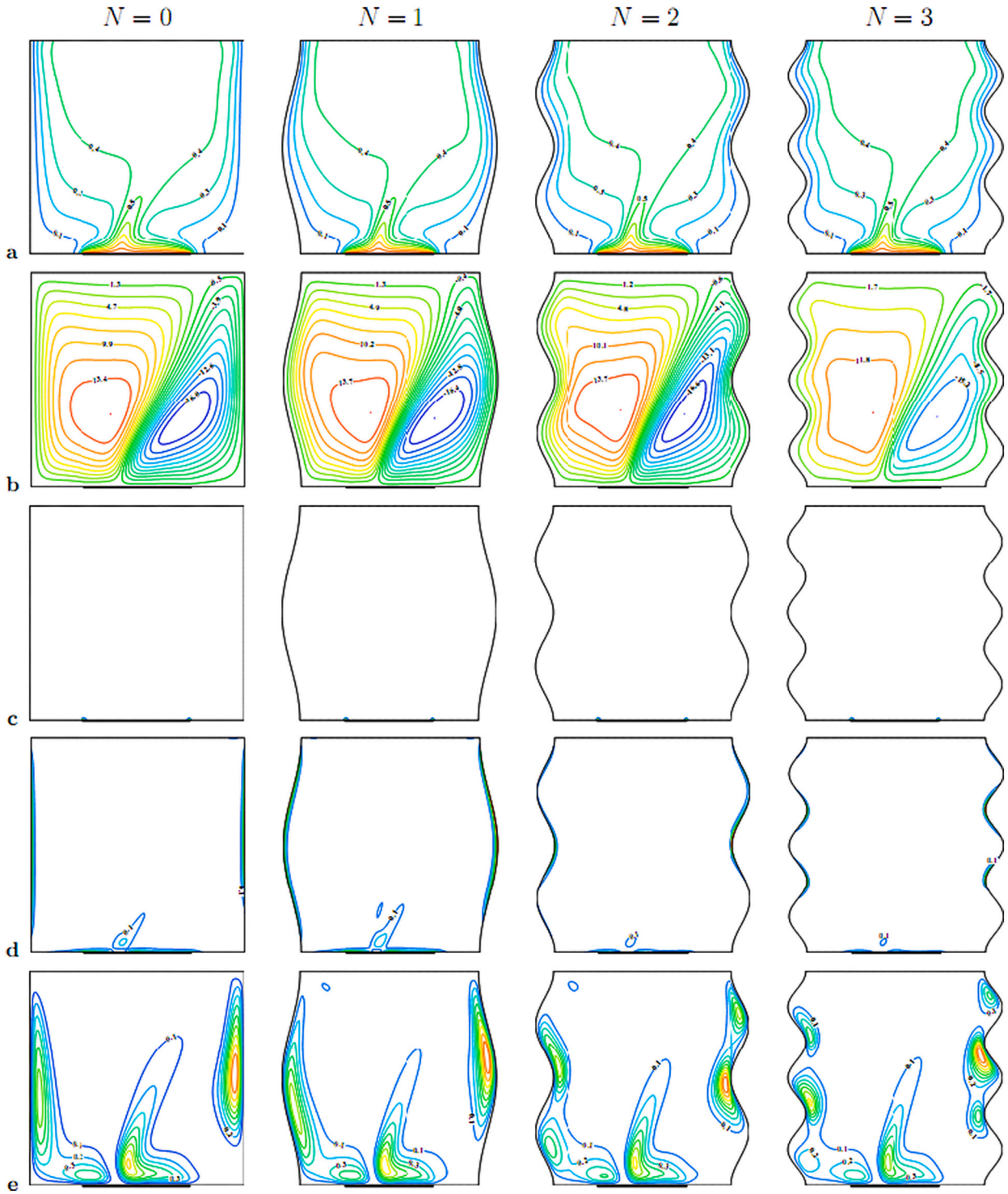

Fig. 4. θ (a), Ψ (b), $S_{l,ht}$ (c), $S_{l,ff}$ (d) and $S_{l,mf}$ (e) for $\phi = 0.04$, $Ha = 50$, $\zeta = 45^{\circ}$ and $\Omega = 0.01$ with different values of N.

flow fields and local entropy production maps is portrayed in Fig. 5 for $\phi = 0.04$, $Ha = 50$, $\zeta = 90^{\circ}$ and $\Omega = 0.01$. It is clearly identified that highly crowded isotherm patterns adjacent to the line source which is owing to the greater temperature gradients narrowing towards the uppermost adiabatic wall. With increasing the value of N, the distorted isolines can only be visible at the corrugated walls of the cavity and flow nature appears to have significant change in the remaining areas. Effect of strong buoyancy force results in the formation of heat plume over the bottom-line source with well distributed clockwise and counter clockwise rotating strong convective cells inside the chamber is observed for $N \geq 0$. Physically, Lorentz force supports the motion of alumina nanoparticles in a vertical direction and consequently, strength of fluid flow rate is manifested particularly at a flat boundary (see Table 8).

It should be noted that the local entropy production due to thermal transfer is found to be less significant when N is increasing which have seen in Fig. 5(c). From the formation of liquid friction, strength of the heat plume and frictional line density in vertical direction get diminished upon increasing N. Magnetic entropy lines are formed as horizontal direction due to the presence of Lorentz force acted in vertical flow regions which have shown in Fig. 5(e). When increasing the

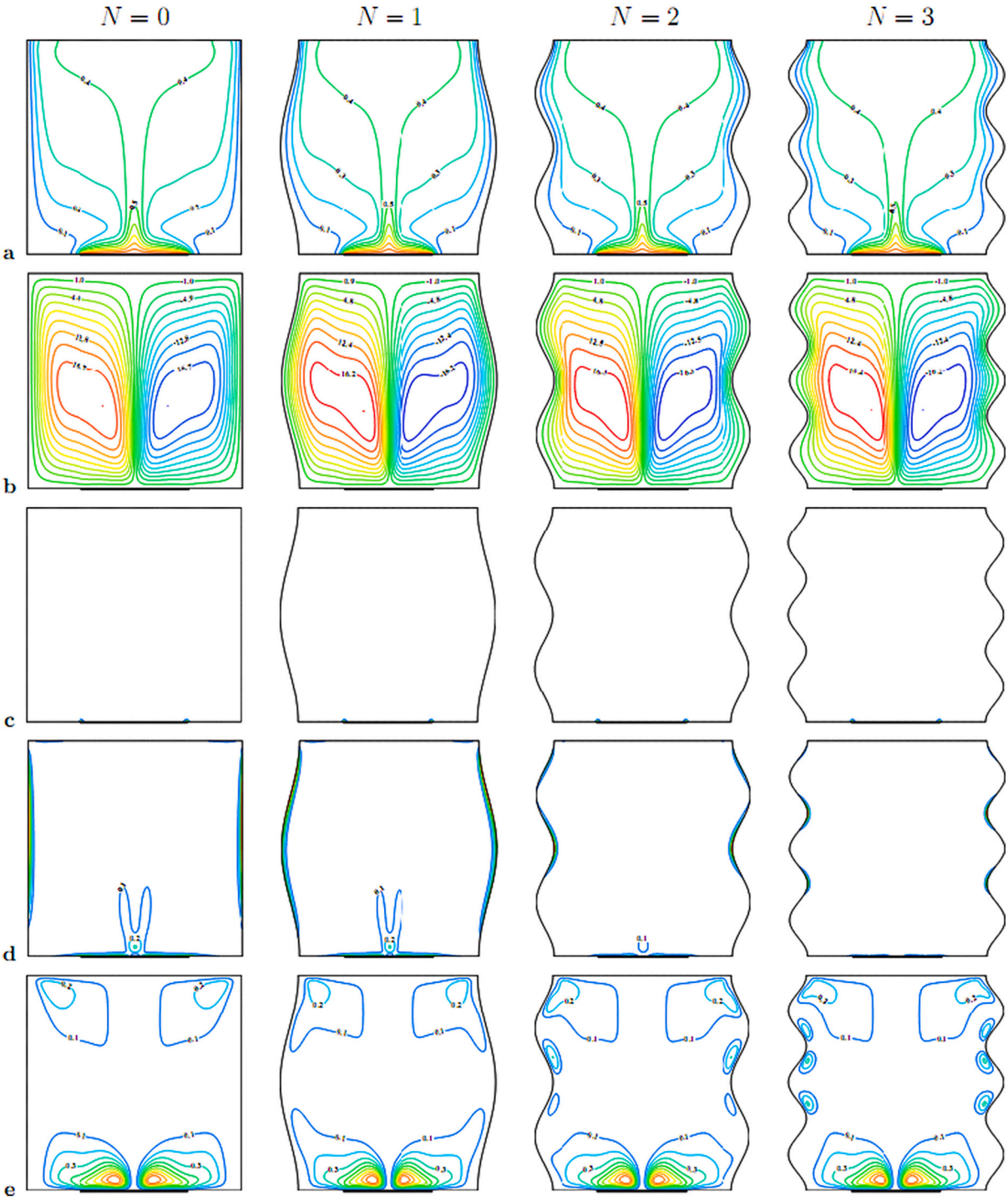

Fig. 5. θ (a), Ψ (b), $S_{l,ht}$ (c), $S_{l,ff}$ (d) and $S_{l,mf}$ (e) for $\phi = 0.04$, $Ha = 50$, $\zeta = 95^{\circ}$ and $\Omega = 0.01$ with different values of N.

undulation parameter ($N \geq 2$), distinctly rotating eddies are made in the vicinity of the corrugated vertical walls owing to an obstruction effect. Moreover, maximum rate of magnetic horizontal lines is monitored over the line source due to the interaction of two sets of recirculating cells as seen from Fig. 3(e).

Fig. 6 represents the relation between Nu_{avg} and ϕ under varying N, Ha and ζ. It is well-known that an inclusion of nanoparticles into the base liquid improves both the heat conductivity and effective viscosity of a base fluid. It should be noted that when increasing the nanoparticle volume fraction along with number of undulations which yields linear increment of Nu_{avg}. It is presumed that when an increase in N from flat wall to wavy wall, result in slowdown of the heat transfer process and consequently, it diminishes Nu_{avg}. The outcomes revealed that maximum rate of heat transfer is manifested for $N = 1$ in the non-zero portions, which makes the fluid particles to travel easily within the entire chamber. Moreover, an increment in magnetic field ($Ha = 50$) leads to suppress the convective heat transfer process and thus, Nu_{avg} can be reduced moderately. Physically, this is because of the impact of Lorentz force controls the heat transfer performance in the entire cavity. Also, it is noticed that for all values of N and ϕ, increasing trend in magnetic inclination angle (ζ) gets higher value of the heat transfer performance. Eventually, it is concluded that convective heat transfer performance is

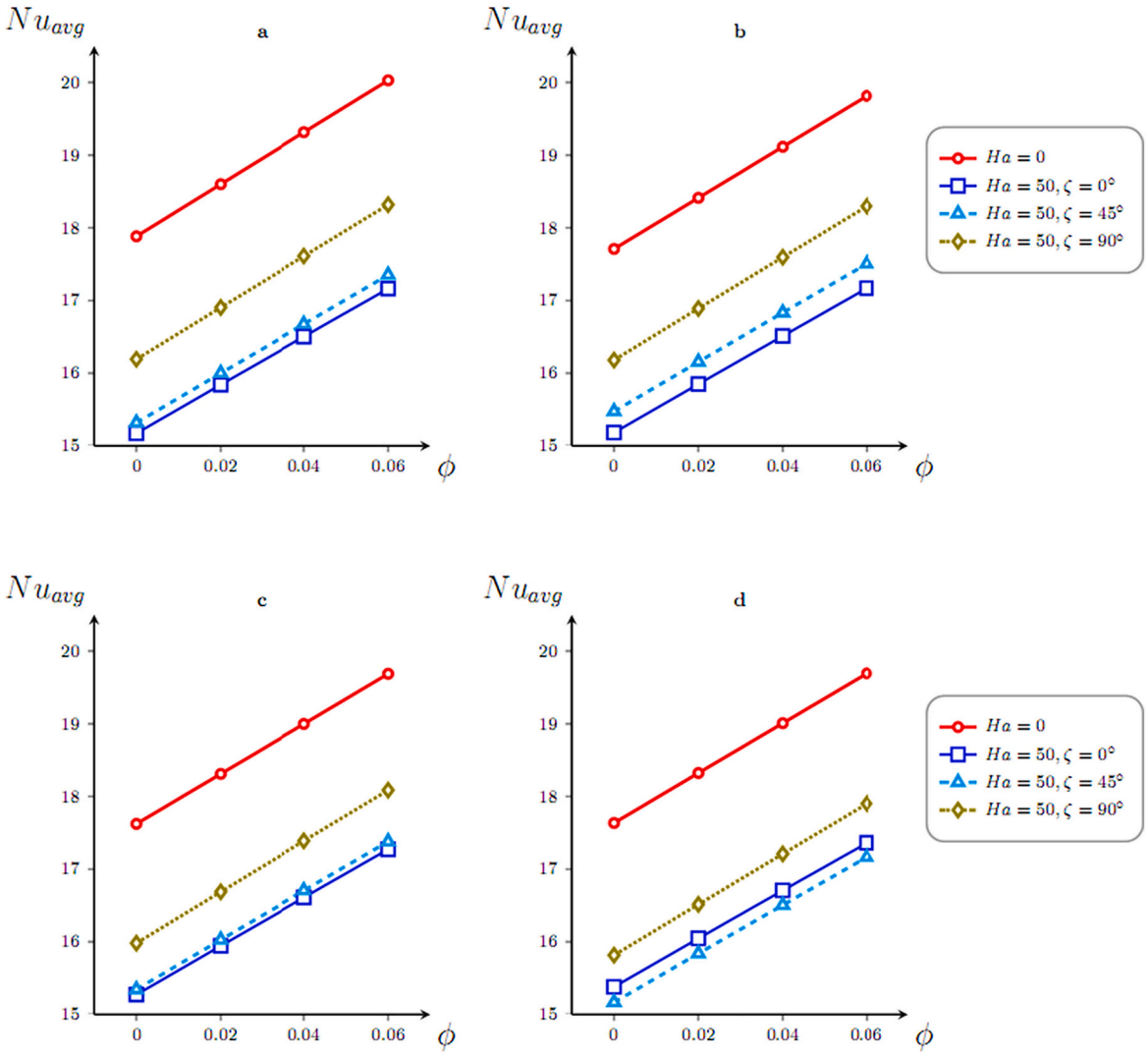

Fig. 6. Variation of Nu_{avg} for $N = 0$ (a), $N = 1$ (b), $N = 2$ (c) and $N = 3$ (d) with ϕ for different Ha and ϕ.

ideal when $Ha = 50$ and $\zeta = 90°$ for all given undulation numbers, because of Lorentz force acts equivalent to the buoyancy effect.

Fig. 7 displays the changes in $S_{l,ht,avg}$, $S_{l,ff,avg}$ and $S_{l,mf,avg}$ versus Ω at ϕ = 0.04 for different values of N, Ha and ζ respectively. It is seen from the plots that the average entropy production caused by $S_{l,ht,avg}$, $S_{l,ff,avg}$ and $S_{l,mf,avg}$ drops when the heat difference (Ω) increases. Since, the corresponding irreversibilities are inversely proportional to the temperature difference. From both thermal and liquid friction entropy production, it is presumed that when the value of Ha is equal to zero, an increasing trend in average entropy production is observed and vice versa. Simultaneously, $S_{l,mf,avg}$ can be found to be maximum when $Ha = 50$ and $\zeta = 0°$. The findings exposed that when the value of N is increasing, the thermal entropy production diminishes gradually. Similar trend is observed for all the values of magnetic inclination angles ($\zeta = 0° - 90°$). In particular, inclined magnetic effect has potential to control the average entropy production rate when $N \geq 2$. As such, presence of magnetic entropy production has a favourable effect in designing a wavy system. It is further reasoned that the strength of the Lorentz force affects the flow field pattern within the cavity and consequently, the average entropy production is limited. Table 8 presents the values of $|\Psi|_{\max}$ and $S_{l,ht,\max}$, $S_{l,ff,\max}$ and $S_{l,mf,\max}$. It is noticed that specific changes are observed for $S_{l,ht,\max}$, while insignificant changes can be found for $S_{l,ff,\max}$ and $S_{l,mf,\max}$.

6. Conclusions

Entropy production on magnetic thermal convective process of alumina-H_2O nanoliquid in either a flat or wavy structured enclosure was numerically investigated. The vertical wavy boundaries are considered at cold temperature T_c and centre of the bottom wall is kept at high temperature T_h, while the upper region and rest of the lower boundary is adiabatic. The governing differential equations are handled by finite volume technique along with power-law differencing scheme. Profiles of isotherms, streamlines and local entropy production owing to thermal transfer, liquid friction and magnetic field for an extensive range of governing parameters have been discussed. The obtained results are accounted as follows:

- An increasing effect of magnetic field weakened the fluid motion rate, average convective Nusselt number and entropy production.
- The average heat transfer and total entropy production can be decreased as the presence of undulation parameter (N) increases. It is also found that the change of number of waves offers a visual variation of the core vortex. A growth of the nanoparticles concentration along with number of undulations enhances the convective heat transfer cum average entropy production. From this study, the outcomes revealed that the maximum value of Nu_{avg} for Al_2O_3-water nanoliquid is $Nu_{avg} = 20.0301$ for $N = 0$ and $Ha = 0$.

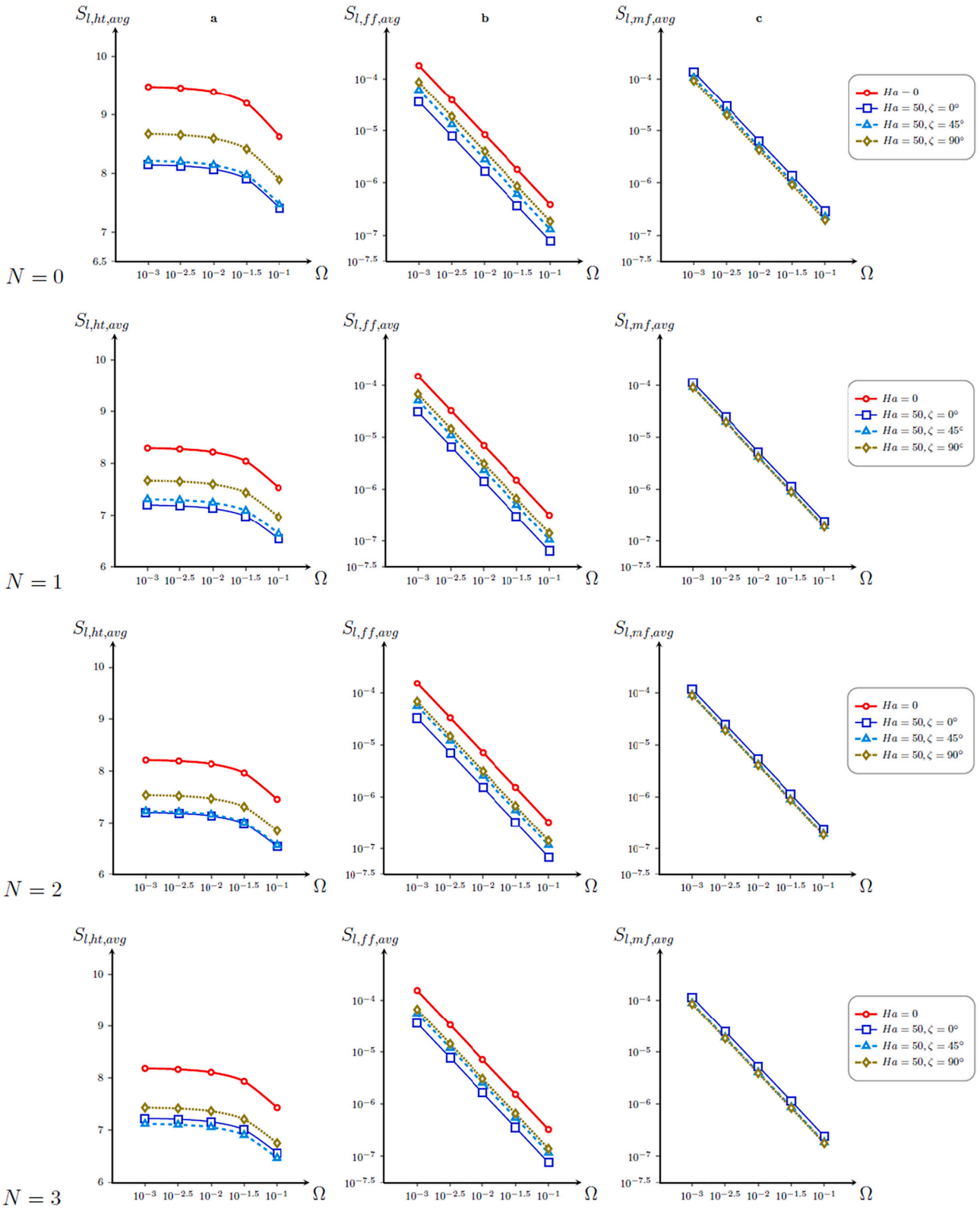

Fig. 7. Variation of average entropy production owing to thermal transfer (a), liquid friction (b) and magnetic impact (c) with Ω for $\phi = 0.04$ and different values of *N*, *Ha* and ζ.

- For all values of *N*, magnetic parameter (*Ha*) and magnetic tilted angle ($\zeta = 0° - 90°$) it is possible to control the behaviour of thermal and flow patterns associated with entropy production caused by thermal transfer, liquid friction and magnetic impact.
- Due to inverse proportionality of temperature difference, an inclusion of the dimensionless temperature difference (Ω) drops the average entropy generation produced by thermal transfer, liquid friction and magnetic impact for all considered values of *N*.

- From the existing outcomes, we concluded that for specified pertinent parameters, the improvement in heat transfer is obtained on flat wall ($N = 0$) while minimizing entropy production is attained by wavy wall ($N = 3$). Thus, the importance of examining the convective features in the wavy formed enclosure can be salient from its applicability to the electronic gadgets and solar collectors.

CRediT authorship contribution statement

C. Sivaraj: Conceptualization, Methodology, Software, Validation, Data curation, Writing – original draft. **S. Gowtham:** Investigation, Software, Validation, Writing – original draft, Writing – review & editing. **M. Elango:** Investigation, Software, Validation, Writing – original draft, Writing – review & editing. **M.A. Sheremet:** Investigation, Writing – original draft, Project administration, Writing – review & editing.

Declaration of Competing Interest

None.

Acknowledgements

This work of C. Sivaraj was carried out as a part of a research project (Grand No: INT/RUS/RFBR/P-282) awarded by the Department of Science and Technology, India. One of the authors (S. Gowtham) thanks the Adi Dravidar and Tribal Welfare Department, Tamil Nadu for its financial support through the full time PhD Scholars incentive scheme. This research of M.A. Sheremet was supported by the Tomsk State University Development Programme (Priority-2030).

References

[1] M. Sheikholeslami, M.G. Bandpy, D.D. Ganji, S. Soleimani, S.M. Seyyadi, Natural convection of nanofluids in an enclosure between a circular and a sinusoidal cylinder in the presence of magnetic field, Int. Commun. Heat Mass Transf. 39 (2012) 1435–1443.
[2] M. Sheikholeslami, M.G. Bandpy, D.D. Ganji, Numerical investigation of MHD effects on Al_2O_3–water nanofluid flow and heat transfer in a semi-annulus enclosure using LBM, Energy 60 (2013) 501–510.
[3] Z. Mehrez, A.E. Cafsi, A. Belghith, P.L. Quéré, MHD effects on heat transfer and entropy generation of nanofluid flow in an open cavity, J. Magn. Magn. Mater. 374 (2015) 214–224.
[4] M.A. Sheremet, I. Pop, N.C. Rosca, Magnetic effect on the unsteady natural convection in a wavy-walled cavity filled with a nanofluid: Buongiorno's mathematical model, J. Taiwan Inst. Chem. Eng. 61 (2016) 211–222.
[5] N. Rudraiah, R.M. Barron, M. Venkatachalappa, C.K. Subbaraya, Effect of a magnetic field on free convection in a rectangular enclosure, Int. J. Eng. Sci. 33 (1995) 1075–1084.
[6] H. Ozoe, K. Okada, The effect of the direction of the external magnetic field on the three-dimensional natural convection in a cubical enclosure, Int. J. Heat Mass Transf. 32 (1989) 1939–1954.
[7] N.M. Al-Najem, K.M. Khanafer, M.M. El-Rafaee, Numerical study of laminar natural convection in tilted enclosure with transverse magnetic field, Int. J. Numer. Method Heat Fluid Flow 8 (1998) 651–672.
[8] J.-H. Jang, W.-M. Yan, Mixed convection heat and mass transfer along a vertical wavy surface, Int. J. Heat Mass Transf. 47 (2004) 419–428.
[9] S. Mahmud, R.A. Fraser, Free convection and entropy generation inside a vertical inphase wavy cavity, Int. Commun. Heat Mass Transf. 31 (2004) 455–466.
[10] B.A.I. Bendrer, A. Abderrahmane, S.E. Ahmed, Z.A.S. Raizah, 3D magnetic buoyancy-driven flow of hybrid nanofluids confined wavy cubic enclosures including multi-layers and heated obstacle, Int. Commun. Heat Mass Transf. 126 (2021) 105431.
[11] R. Nasrin, S. Parvin, Hydromagnetic effect on mixed convection in a lid-driven cavity with sinusoidal corrugated bottom surface, Int. Commun. Heat Mass transf. 38 (2011) 781–789.
[12] Md.F.A. Asad, Md.N. Alam, A.M. Rashad, Md.M.A. Sarker, Impact of undulation on magneto-free convective heat transport in an enclosure having vertical wavy sides, Int. Commun. Heat Mass Transf. 127 (2021) 105579.
[13] P.S. Rao, P. Barman, Natural convection in a wavy porous cavity subjected to a partial heat source, Int. Commun. Heat Mass transf. 120 (2021) 105007.
[14] P. Barman, P.S. Rao, Effect of aspect ratio on natural convection in a wavy porous cavity submitted to a partial heat source, Int. Commun. Heat Mass transf. 126 (2021) 105453.
[15] S.G. Martyushev, M.A. Sheremet, Conjugate natural convection combined with surface thermal radiation in an air filled cavity with internal heat source, Int. J. Therm. Sci. 76 (2014) 51–67.
[16] H.F. Oztop, P. Estellé, W.M. Yan, K. Al-Salem, J. Orfi, O. Mahian, A brief review of natural convection in enclosures under localized heating with and without nanofluids, Int. Commun. Heat Mass Transf. 60 (2015) 37–44.
[17] G. Saha, Finite element simulation of magnetoconvection inside a sinusoidal corrugated enclosure with discrete isoflux heating from below, Int. Commun. Heat Mass Transf. 37 (2010) 393–400.
[18] S.U.S. Choi, Enhancing thermal conductivity of fluids with nanoparticles, in: D. A. Siginer, H.P. Wang (Eds.), Developments and Applications of Non-Newtonian Flows, ASME, FED-231/MD-66, 1995, pp. 99–105.
[19] H.F. Oztop, E. Abu-Nada, Y. Varol, A. Chamkha, Natural convection in wavy enclosures with volumetric heat sources, Int. J. Therm. Sci. 50 (2011) 502–514.
[20] D. Das, M. Roy, T. Basak, Studies on natural convection within enclosures of various (non-square) shapes – a review, Int. J. Heat Mass Transf. 106 (2017) 356–406.
[21] T. Grosan, M.A. Sheremet, I. Pop, Heat transfer enhancement in cavities filled with nanofluids, in: A.A. Minea (Ed.), Advances Heat Transfer Fluids: from Numerical to Experimental Techniques, CRC Press, Taylor & Francis, New York, 2017, pp. 267–284.
[22] O. Mahian, L. Kolsi, M. Amani, P. Estellé, G. Ahmadi, C. Kleinstreuer, J.S. Marshall, M. Siavashi, R.A. Taylor, H. Niazmand, S. Wongwises, T. Hayat, A. Kolanjiyil, A. Kasaeian, I. Pop, Recent advances in modeling and simulation of nanofluid flows-part I: fundamental and theory, Phys. Rep. 790 (2018) 1–48.
[23] M.U. Sajid, H.M. Ali, Recent advances in application of nanofluids in heat transfer devices: a critical review, Renew. Sust. Energ. Rev. 103 (2019) 556–592.
[24] M. Uddin, W. Khan, S. Qureshi, O.A. Bég, Bioconvection nanofluid slip flow past a wavy surface with applications in nano-biofuel cells, Chin. J. Phys. 55 (5) (2017) 2048–2063.
[25] R.A. Burton, G.B. Fincher, Plant cell wall engineering: applications in biofuel production and improved human health, Curr. Opin. Biotechnol. 26 (2014) 79–84.
[26] M.A. Sheremet, Applications of Nanofluids, Nanomaterials 11 (2021) 1716.
[27] U. Khan, A. Zaib, I. Khan, K.S. Nisar, Insight into the dynamics of transient blood conveying gold nanoparticles when entropy generation and Lorentz force are significant, Int. Commun. Heat Mass Transf. 127 (2021) 105415.
[28] N. Acharya, A.J. Chamkha, On the magnetohydrodynamic Al_2O_3-water nanofluid flow through parallel fins enclosed inside a partially heated hexagonal cavity, Int. Commun. Heat Mass Transf. 132 (2022) 105885.
[29] S.K. Das, S.U.S. Choi, W. Yu, Y. Predeep, Nanofluids: Science and Technology, Wiley, New Jersey, 2008.
[30] A. Shenoy, M. Sheremet, I. Pop, Convective Flow and Heat Transfer from Wavy Surfaces: Viscous Fluids, Porous Media and Nanofluids, CRC Press, Taylor & Francis Group, New York, 2016.
[31] E. Abu-Nada, H.F. Oztop, Numerical analysis of Al_2O_3/water nanofluids natural convection in a wavy walled cavity, Numer. Heat Transf. 59 (2011) 403–419.
[32] C.C. Cho, C.L. Chen, C.K. Chen, Natural convection heat transfer performance in complex-wavy-wall enclosed cavity filled with nanofluid, Int. J. Therm. Sci. 60 (2012) 255–263.
[33] M. Nikfar, M. Mahmoodi, Meshless local Petrov-Galerkin analysis of free convection of nanofluid in a cavity with wavy side walls, Eng. Anal. Bound. Element 36 (2012) 433–445.
[34] M.A. Sheremet, H.F. Oztop, I. Pop, MHD natural convection in an inclined wavy cavity with corner heater filled with a nanofluid, J. Magn. Magn. Mater. 416 (2016) 37–47.
[35] M.A. Sheremet, I. Pop, H.F. Oztop, N. Abu-Hamdeh, Natural convective heat transfer and nanofluid flow in a cavity with top wavy wall and corner heater, J. Hydrodyn. 28 (2016) 873–885.
[36] H.F. Oztop, A. Sakhrieh, E. Abu-Nada, K. Al-Salem, Mixed convection of MHD flow in nanofluid filled and partially heated wavy walled lid-driven enclosure, Int. Commun. Heat Mass Transf. 86 (2017) 42–51.
[37] M.A. Sheremet, R. Trimbitas, T. Grosan, I. Pop, Natural convection of an alumina-water nanofluid inside an inclined wavy-walled cavity with a non-uniform heating using Tiwari and Das' nanofluid model, Appl. Math. Mech. 39 (2018) 1425–1436.
[38] M.J. Uddin, S.K. Rasel, M.M. Rahman, K. Vajravelu, Natural convective heat transfer in a nanofluid-filled square vessel having a wavy upper surface in the presence of a magnetic field, Therm. Sci. Eng. Prog. 19 (2020) 100660.
[39] Y. Chen, P. Luo, Q. Tao, X. Liu, D. He, Natural convective heat transfer investigation of nanofluids affected by electrical field with periodically changed direction, Int. Commun. Heat Mass Transf. 128 (2021) 105613.
[40] A. Bejan, A study of entropy generation in fundamental convective heat transfer, ASME J. Heat Transf. 101 (1979) 718–725.
[41] A. Bejan, Entropy Generation through Heat and Fluid Flow, Wiley, New York, 1982.
[42] A. Bejan, Entropy Generation Minimization: The Method of Thermodynamic Optimization of Finite-Size Systems and Finite-Time Processes, CRC Press, Boca Raton, 1996.
[43] H.F. Oztop, K. Al-Salem, A review on entropy generation in natural and mixed convection heat transfer for energy systems, Renew. Sust. Energ. Rev. 16 (2012) 911–920.
[44] O. Mahian, A. Kianifar, C. Kleinstreuer, M.A. Al-Nimr, I. Pop, A.Z. Sahin, S. Wongwises, A review of entropy generation in nanofluid flow, Int. J. Heat Mass Transf. 65 (2013) 514–532.
[45] S. Mahmud, A.K.M.S. Islam, Laminar free convection and entropy generation inside an inclined wavy enclosure, Int. J. Therm. Sci. 42 (2003) 1003–1012.

[46] C.C. Cho, Heat transfer and entropy generation of natural convection in nanofluid-filled square cavity with partially-heated wavy surface, Int. J. Heat Mass Transf. 77 (2014) 818–827.
[47] S. Kashani, A.A. Ranjbar, M. Mastiani, H. Mirzaei, Entropy generation and natural convection of nanoparticle-water mixture (nanofluid) near water density inversion in an enclosure with various patterns of vertical wavy walls, Appl. Math. Comput. 226 (2014) 180–193.
[48] S. Bhardwaj, A. Dalal, S. Pati, Influence of wavy wall and non-uniform heating on natural convection heat transfer and entropy generation inside porous complex enclosure, Energy 79 (2015) 467–481.
[49] R. Parveen, T.R. Mahapatra, Numerical simulation of MHD double diffusive natural convection and entropy generation in a wavy enclosure filled with nanofluid with discrete heating, Heliyon 5 (2019), e02496.
[50] A.S. Dogonchi, M.S. Sadeghi, M. Ghodrat, A.J. Chamkha, Y. Elmasry, R. Alsulami, Natural convection and entropy generation of a nanoliquid in a crown cavity: effect of thermo-physical parameters and cavity shape, Case Stud. Therm. Eng. 27 (2021) 101208.
[51] S. Munawar, N. Saleem, W.A. Khan, Entropy generation minimization E.G.M. analysis of free convective hybrid nanofluid flow in a corrugated triangular annulus with a central triangular heater, Chin. J. Phys. 75 (2022) 38–54.
[52] C.C. Cho, Effects of porous medium and wavy surface on heat transfer and entropy generation of Cu-water nanofluid natural convection in square cavity containing partially-heated surface, Int. Commun. Heat Mass Transf. 119 (2020) 104925.
[53] W. Chammam, S. Nazari, S.Z. Abbas, Numerical scrutiny of entropy generation and ferro-nanoliquid magnetic natural convection inside a complex enclosure subjected to thermal radiation, Int. Commun. Heat Mass Transf. 125 (2021) 105319.
[54] Z. Korei, S. Benissaad, F. Berrahil, A. Filali, MHD mixed convection and irreversibility analysis of hybrid nanofluids in a partially heated lid-driven cavity chamfered from bottom side, Int. Commun. Heat Mass Transf. 132 (2022) 105895.
[55] C. Sivaraj, M.A. Sheremet, MHD natural convection and entropy generation of ferrofluids in a cavity with a non-uniformly heated horizontal plate, Int. J. Mech. Sci. 149 (2018) 326–337.
[56] T. Javed, M.A. Siddiqui, Effect of MHD on heat transfer through ferrofluid inside a square cavity containing obstacle/heat source, Int. J. Therm. Sci. 125 (2018) 419–427.
[57] C. Sivaraj, E. Vignesh, M.A. Sheremet, Thermogravitational convection of ferrofluid combined with the second law of thermodynamics for an open chamber with a heat generating solid block under an influence of uniform magnetic field, Int. Commun. Heat Mass Transf. 129 (2021) 105712.
[58] B.C. Pak, Y.I. Cho, Hydrodynamic and heat transfer study of dispersed fluids with submicron metallic oxide particles, Exp. Heat Transf. 11 (2) (1998) 151–170.
[59] Y. Xuan, W. Roetzel, Conceptions for heat transfer correlation of nanofluids, Int. J. Heat Mass Transf. 43 (2000) 3701–3707.
[60] H.C. Brinkman, The viscosity of concentrated suspensions and solutions, J. Chem. Phys. 20 (1952) 571.
[61] T. Armaghani, A. Kasaeipoor, N. Alavi, M.M. Rashidi, Numerical investigation of water-alumina nanofluid natural convection heat transfer and entropy generation in a baffled L-shaped cavity, J. Mol. Liq. 223 (2016) 243–251.
[62] S. Priyadharsini, C. Sivaraj, Numerical simulation of thermo-magnetic convection and entropy generation in a ferrofluid filled square chamber with effects of heat generating solid body, Int. Commun. Heat Mass Transf. 131 (2022) 105753.
[63] B. Calcagni, F. Marsili, M. Paroncini, Natural convective heat transfer in square enclosures heated from below, Appl. Therm. Eng. 25 (2005) 2522–2531.
[64] O. Aydin, W.J. Yang, Natural convection in enclosures with localized heating from below and symmetrical cooling from sides, Int. J. Numer. Method Heat Fluid Flow 10 (2000) 518–529.
[65] B. Ghasemi, S.M. Aminossadati, A. Raisi, Magnetic field effect on natural convection in a nanofluid-filled square enclosure, Int. J. Therm. Sci. 50 (2011) 1748–1756.
[66] M. Magherbi, H. Abbassi, A. Ben Brahim, Entropy generation at the onset of natural convection, Int. J. Heat Mass Transf. 46 (2003) 3441–3450.
[67] C.C. Cho, C.H. Chiu, C.Y. Lai, Natural convection and entropy generation of Al_2O_3–water nanofluid in an inclined wavy-wall cavity, Int. J. Heat Mass Transf. 97 (2016) 511–520.